EDGE ELEMENT MODELING OF 3D INTERCONNECTION STRUCTURES

†Jilin Tan, Guangwen Pan, and *Barry K. Gilbert
†Compact Software Inc., Arizona State University, *Mayo Foundation

ABSTRACT

In this paper, we apply the local potential concept to construct a functional for the finite element method (FEM) with 3D structures. The corresponding boundary conditions at the planes of incidence and transmittance for hybrid modes are derived. These conditions take into account both the transverse and longitudinal field components of the propagating signals. Employing these boundary conditions, in conjunction with the absorbing boundary conditions (ABC) and/or the boundary conditions of the first and third kind, a 3D asymmetrical functional is implemented as a hybrid vector edge element method. Numerical examples are presented for air bridges and lossy transmission lines, connected by a through-hole via. The equivalent frequency dependent circuit parameters are then extracted from the field solutions. Laboratory measurements and data comparison with previous published results strongly support the newly developed theoretical work.

INTRODUCTION

In recent years, millimeter wave integrated circuits, very large scale integrated (VLSI) circuits and integrated opto-electronics, have undergone extremely rapid development. This rapid evolution has in turn expanded the interest in, and expectations of, the modeling and analysis of guided wave structures at both the electromagnetic (EM) field and equivalent circuit levels. The full-wave EM modeling and simulation of 3D lossy structures have become a necessity in the design and optimization of state-of-the-art systems.

In this paper, we have developed a new functional for general 3D guided wave structures, which need not have completely closed metallic walls. We shall then derive the termination conditions at the plane of incidence and the plane of transmittance. This 3D asymmetrical functional is then implemented by using hybrid vector finite elements. Utilizing prior information of the eigenmodes resulting from the evaluation of the $2\frac{1}{2}$D edge element solver [1], the 3D field solutions are obtained. The frequency dependent circuit parameters, such as L, C, R, G, are converted according to relevant equivalent circuits of the structures.

BASIC THEORY

In the finite element implementation, the basic EM equation, which is to be solved for the 3D structures in a full-wave analysis, is the vector wave propagation equation

$$\nabla \times \frac{1}{\mu_r} \nabla \times \vec{E} - \vec{\bar{\epsilon}}_r k_0^2 \cdot \vec{E} = -j\omega\mu\vec{J} \quad \text{in } V \qquad (1)$$

The boundary conditions for (1) are

$$\begin{cases} \hat{n} \times \vec{E} = \vec{P} & \text{on } S_1 \\ \frac{1}{\mu_r} \hat{n} \times \nabla \times \vec{E} + \gamma_v \hat{n} \times \hat{n} \times \vec{E} = \vec{V} & \text{on } S_2 \end{cases} \qquad (2)$$

In the previous equations, S_1 is the surface where the boundary condition of the first kind applies, and S_2 the surface where the boundary condition of the third kind applies, and $\gamma_v = jk_0\sqrt{\frac{\epsilon_{rc} - j\frac{\sigma}{\omega\epsilon_0}}{\mu_{rc}}}$, as defined in [1]. The boundary condition of the second kind can be included within the third kind. In the application of this theory to transmission line structures and their discontinuities, the field component in the signal propagation direction is generally nonzero, and the aforementioned boundary conditions are insufficient. On both the incident and transmitted planes, the longitudinal component needs to be treated carefully [2]. Without losing generality, we will employ a typical

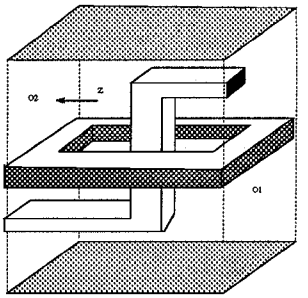

Fig. 1. Via configuration

via structure as an example. On the incident plane O_1 and transmitted plane O_2, the suitable termination condition is found to be

$$\hat{n} \times \nabla \times \vec{E} + \gamma_p \hat{n} \times \hat{n} \times [\vec{E} + \frac{\nabla_t E_n}{\gamma_p}] = \vec{U} \qquad (3)$$

Generally, the functional is no longer symmetric because of (3). Furthermore, to be consistent with the treatment in the $2\frac{1}{2}$D case, and with the expressions that we proposed in [1], the adjoint field should be the field which is incident upon plane O_2 and transmitted through O_1. This adjoint system satisfies

$$\nabla \times \frac{1}{\mu_r} \nabla \times \vec{E}^{\dagger} - \vec{\bar{\epsilon}}_r k_0^2 \cdot \vec{E}^{\dagger} = -j\omega\mu \vec{J}^{\dagger} \quad \text{in } V \quad (4)$$

under the associated boundary conditions

$$\begin{cases} \hat{n} \times \vec{E}^{\dagger} = \vec{P}^{\dagger} \\ \frac{1}{\mu_r} \hat{n} \times \nabla \times \vec{E}^{\dagger} + \gamma_v^{\dagger} \hat{n} \times \hat{n} \times \vec{E}^{\dagger} = \vec{V}^{\dagger} \\ \hat{n} \times \nabla \times \vec{E}^{\dagger} + \gamma_p^{\dagger} \hat{n} \times \hat{n} \times [\vec{E}^{\dagger} + \frac{\nabla_t E_n^{\dagger}}{\gamma_p^{\dagger}}] = \vec{U}^{\dagger} \end{cases} \quad (5)$$

Suppose that we can find an $\vec{E}_0$ or $\vec{E}_0^{\dagger}$ which satisfies the aforementioned boundary conditions. If we define $\vec{e} = \vec{E} - \vec{E}_0$, then the following functional [3]

$$I = < \vec{e}^{\dagger}, \hat{L}\vec{e} > - < \vec{e}^{\dagger}, \vec{j} > - < \vec{e}, \vec{j}^{\dagger} > \quad (6)$$

can still apply provided that the assumed known vector $\vec{U}$ is modified to $\vec{U} - \hat{n} \times \hat{n} \times \nabla_t E_n$ and the local potential method is employed. Following similar procedures presented in [4], we may further simplify the functional, yielding

$$\begin{aligned} I &= \int_V [\frac{1}{\mu_r} (\nabla \times \vec{E}^{\dagger}) \cdot (\nabla \times \vec{E}) - k_0^2 \vec{E}^{\dagger} \cdot \vec{\bar{\epsilon}}_r \cdot \vec{E}] dv \\ &+ \int_{S_2} \gamma_v (\hat{n} \times \vec{E}^{\dagger}) \cdot (\hat{n} \times \vec{E}) ds \\ &+ \int_{O_1+O_2} \frac{\gamma_p}{\mu_r} (\hat{n} \times \vec{E}^{\dagger}) \cdot (\hat{n} \times \vec{E}) ds \\ &+ \int_{O_1+O_2} \frac{1}{\mu_r} (\vec{U}_0 \cdot \vec{E}^{\dagger} + \vec{U}_0^{\dagger} \cdot \vec{E}) ds \\ &+ \int_{S_2} (\vec{V} \cdot \vec{E}^{\dagger} + \vec{V}^{\dagger} \cdot \vec{E}) ds \\ &+ j\omega\mu_0 \int_V (\vec{j} \cdot \vec{E}^{\dagger} + \vec{j}^{\dagger} \cdot \vec{E}) dv \end{aligned} \quad (7)$$

Eq. (7) can be verified by using Galerkin's procedure to transform the vector wave equation into the weak integral form [1]. For the via structure, the incident field can be expressed as $\vec{E}_{in} = \vec{E}^0(x,y)e^{-\gamma(z-z_1)}$ on the plane of incidence O_1. Thus

$$\begin{aligned} \vec{E} &= \vec{E}_t^0(x,y)e^{-\gamma_1(z-z_1)} + \Gamma \vec{E}_t^0(x,y)e^{\gamma_1(z-z_1)} \\ &+ \vec{E}_z^0(x,y)e^{-\gamma_1(z-z_1)} - \Gamma \vec{E}_z^0(x,y)e^{\gamma_1(z-z_1)} \\ &= \vec{E}^{in} + \vec{E}^{re} \end{aligned} \quad (8)$$

where Γ is the reflection coefficient. Consequently, on this surface we obtain

$$\begin{aligned} & \hat{n} \times \nabla \times \vec{E} + \gamma_1 \hat{n} \times \hat{n} \times \vec{E} \\ = \; & 2\gamma_1 \hat{n} \times \hat{n} \times \vec{E}^{in} - \hat{n} \times \hat{n} \times \nabla_t E_n \\ = \; & \vec{U}_0 \end{aligned} \quad (9)$$

Note that γ_1 in (8) is the complex propagation constant for the $2\frac{1}{2}D$ uniform line case, which has been obtained from the precomputation of the $2D\frac{1}{2}$ edge element codes. Comparing (9) with (3), we have

$$\begin{cases} \gamma_p = \gamma_1 \\ \vec{U} = 2\gamma_1 \hat{n} \times (\hat{n} \times \vec{E}^{in}) \end{cases} \quad (10)$$

On O_2, the surface through which the wavefront propagates out of the via structure, we have

$$\begin{aligned} \vec{E} &= T\vec{E}^0(x,y)e^{-\gamma_2(z-z_2)} \\ &= \vec{E}^{tr} \end{aligned} \quad (11)$$

where T is the transmission coefficient. On O_2, we also have

$$\begin{aligned} & \hat{n} \times \nabla \times \vec{E} + \gamma_2 \hat{n} \times \hat{n} \times \vec{E} \\ = \; & -\hat{n} \times \hat{n} \times \nabla_t E_n \\ = \; & \vec{U}_0 \end{aligned} \quad (12)$$

Therefore, $\gamma_p = \gamma_2$, and $\vec{U} = 0$. On other boundary surfaces, either the boundary conditions of the first or third kind apply. The adjoint field, which satisfies (4) and (5), on O_2 and has the form of $\vec{E}_{in}^{\dagger} = \vec{E}_0^{\dagger} e^{\gamma(z-z_2)}$. At port 2, we have

$$\begin{aligned} \vec{E}^{\dagger} &= \vec{E}_t^0(x,y)e^{\gamma_2(z-z_2)} + R\vec{E}_t^0(x,y)e^{-\gamma_2(z-z_2)} \\ &- \vec{E}_z^0(x,y)e^{\gamma_2(z-z_2)} + R\vec{E}_z^0(x,y)e^{-\gamma_2(z-z_2)} \\ &= \vec{E}^{in\dagger} + \vec{E}^{re\dagger} \end{aligned} \quad (13)$$

Similar to (9), we find

$$\begin{aligned} & \hat{n} \times \nabla \times \vec{E}^{\dagger} + \gamma_2 \hat{n} \times \hat{n} \times \vec{E}^{\dagger} \\ = \; & 2\gamma_2 \hat{n} \times \hat{n} \times \vec{E}^{in\dagger} - \hat{n} \times \hat{n} \times \nabla_t E_n^{\dagger} \\ = \; & \vec{U}_0^{\dagger} \end{aligned} \quad (14)$$

On O_1, the adjoint field is governed by

$$\begin{aligned} & \hat{n} \times \nabla \times \vec{E}^{\dagger} + \gamma_1 \hat{n} \times \hat{n} \times \vec{E}^{\dagger} \\ = \; & -\hat{n} \times \hat{n} \times \nabla_t E_n^{\dagger} \\ = \; & \vec{U}_0^{\dagger} \end{aligned} \quad (15)$$

Two issues related to the functional (7) should be emphasized:

1. The functional (7) will reduce to the form proposed in [1] for uniform $2\frac{1}{2}D$ structures.
2. The $\nabla_t E_n$ term is assumed to be a known function. We will maintain this dual characteristic until the optimization of the functional has been completed.

EDGE ELEMENT PROCEDURE

For reasons of simplicity, the isotropic case will be considered first. We shall assume that the same shape functions employed for the primary fields can also be used for the adjoint fields. For the edge element with a basic building block, we may express the electrical fields in each small cell as [4]

$$\vec{E}^e = \sum_{i=1}^{12} \vec{N}_i^e E_i^e \tag{16}$$

After using the Ritz procedure and grouping together all of the relationships in the global coordinate system, we arrive at

$$\{[Z_v^e]+\gamma[Z_z^s]+[Z_{tz}^s]+[Z_{-tz}^s]+\gamma[Z_{(-z)}^s]+\gamma_p[Z_i^g]\}[E]$$

$$= 2\gamma[Z_z^u][E_t^{in}] \tag{17}$$

Once (17) has been solved, the distribution of the electrical fields will be obtained. The S parameters, including the reflection and transmission coefficients, can be found through the definitions extracted in Eqs. (8, 11). The desired circuit parameters, C, L, R, G, can then be found from network theory.

EXCESS CAPACITANCE AND INDUCTANCE

Once the distribution of the three-dimensional electrical field has been determined, the reflection coefficient can be evaluated from (8). For example, when the system is excited from port 1, we have

$$\Gamma = \frac{\int_{S1} ds[\vec{E}\cdot\vec{E}^{2D} - \vec{E}^{2D}\cdot\vec{E}^{2D}]}{\int_{S1} ds\vec{E}^{2D}\cdot\vec{E}^{2D}} \mid_{z=z_1} \tag{18}$$

Similarly from Eq. (11), the transmission coefficient is

$$T = \frac{\int_{S_2} ds\vec{E}\cdot\vec{E}^{2D}}{\int_{S_2} ds\vec{E}^{2D}\cdot\vec{E}^{2D}} \mid_{z=z_2} \tag{19}$$

provided the field is properly normalized [5]. The scattering parameters of a two-port system are

$$\begin{cases} S_{11} = \Gamma \\ S_{21} = T \end{cases} \tag{20}$$

The Y-parameters can be found from two-port network theoryr. Then, based on the Π type equivalent circuits, we have the equivalent capacitance and inductance

$$\begin{cases} C = \frac{\Im Y_{12}}{\omega} \\ L = \frac{1}{\omega\Im(Y_{11}-Y_{12})}. \end{cases} \tag{21}$$

The resistance and the conductance can be found in the same way. The resistance can be ignored in this equivalent circuit because, while the vias are of fairly small cross section, their vertical height between layers is also quite small (typical via diameters and height are in the range of $30-90\mu m$).

The excess capacitance and inductance can be obtained from (21) by subtracting the 2D uniform line parameters multiplied by the distance inclosed in the structure box.

NUMERICAL EXAMPLES

The non-symmetric complex sparse system equation (17) was solved using the Harwell subroutines. Only a few minutes are required on an IBM 6000 computer for each frequency point, when the total number of unknowns is approximately 3000.

Example 1: An Air Bridge. Air bridges, as depicted in Figure 2, are employed in several high performance integrated circuit technologies to assure minimum interconnect capacitance and maximum signal propagation velocity along the interconnect. The dimension in microns are: $a = 212$, $b = 106$, $w' = 212$, $h_3 = 200$, $h_2 = 60$, $h_1 = 635$, $g = 635$, $w = 635$. The conducting line and the ground plane were assumed in this example to be copper, although in actuality aluminum or gold are typically employed. Our assumption of copper metallurgy in the example allowed us to compare our numerical results with results already published in the literature, which also postulated the use of copper. However, the ohmic loss in this structure was found not to be significant after analyzing and comparing the real-world interconnect with an ideal lossless structure of equivalent geometry. Figure 2 also depicts the scattering parameters evaluated from this method, and from the spectral domain analysis (SDA) method [6]. Results from the two methods show excellent agreement.

Example 2: Via Structure. Through-hole vias are typically used to connect signal lines residing on different metal layers in most printed circuit board technologies and in some multichip module (MCM) technologies. For the circuit design, engineers are concerned about overall signal integrity on interconnects

Reflection & Transmission Coefficients				
GHz	Reflect	Trans	L (nH)	C (pF)
5	2.56E-3	0.99998	55.767E-3	21.274E-3
10	1.29E-2	0.99986	55.568E-3	24.602E-3
15	2.07E-2	0.99968	55.406E-3	24.965E-3
20	2.77E-2	0.99944	55.204E-3	25.046E-3
25	3.46E-2	0.99910	54.95E-3	25.122E-3
30	4.19E-2	0.99876	54.65E-3	25.254E-3

carrying wideband signals, and thus wish to understand the magnitude of the excess inductance and excess capacitance caused by this via discontinuity. The method described herein provides the needed parametric values. Note in the following table that the two reference planes incorporated into the via structure, shown in Fig. 1, are placed at locations $z_1 = 0$ and $z_2 = 0.14\ mm$ respectively. Fig. 3 depicts the side and top view of the structure, with all dimensions (in microns) included. The resulting frequency dependent S-parameters are listed in Table 1. It can be seen from the table that the effect of the via of Fig. 1 to the signal integrity is very minor. Laboratory measurements support this conclusion. The capacitance values are compared with the FDTD results with discrepancy $\leq 7\%$. It appears from this set of data that the new method allows the use of a minimum number of brick edge elements (2000), while nonetheless obtaining a numerically acceptable result.

CONCLUSIONS

In this paper, we have identified an additional term in the boundary condition of the third kind for three dimensional structures. In conjunction with the two dimensional uniform transmission line results, the newly developed three dimensional formulation can extract from impedance discontinuities the reflected and transmitted waves, and convert them into frequency dependent lumped circuit parameters. A numerical example of a through-hole via, typically found in printed circuit boards and multichip modules, was analyzed. As another example, a three dimensional air bridge, a structure employed in some integrated circuit fabrication technologies, was also analyzed. Comparisons with available published results indicate excellent agreement with this new method.

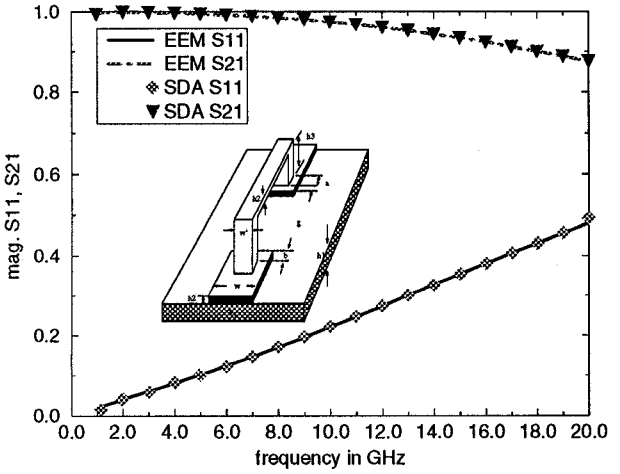

Fig. 2. Scattering parameters for an air bridge

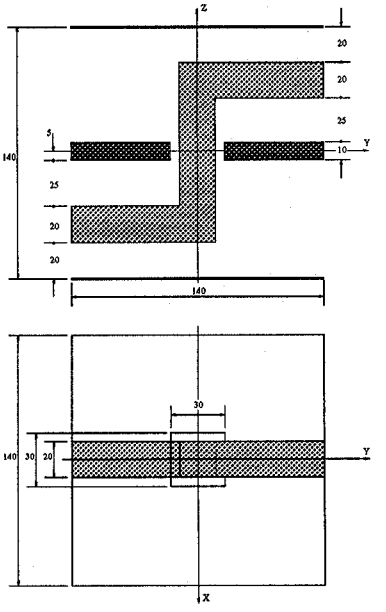

Fig. 3. Side and Top Views of the Through-Hole Via

REFERENCES

[1] J. Tan and G. Pan, "A New Edge Element Analysis of Dispersive Waveguiding Structures," *IEEE, Trans. Microwave Theory Tech.*, vol. 43, no. 11, pp. 2600-2607, Nov. 1995.

[2] J. Wang and R. Mittra, "Finite Element Analysis of MMIC Structures and Electronic Packages Using Absorbing Boundary Conditions," *IEEE, Trans. Microwave Theory Tech.*, vol. 42, no. 3, pp 441-449, March 1994.

[3] W. C. Chew, *Waves and Fields in Inhomogeneous Media*, New York: van Nostrand Reinhold, 1990.

[4] Jianming Jin, *The Finite Element Methods in Electromagnetics*, John Wiley & Sons, Inc., 1993.

[5] R. E. Collin, *Field Theory of Guided Waves*, second edition, IEEE Press, 1990.

[6] T. B. Becks and I. Wolff, "Analysis of 3-D Metalization Structures by a Full-Wave Spectral Domain Technique," *IEEE, Trans. Microwave Theory Tech.*, vol. 40, no. 12, Dec. 1992.